

## Data-Driven Learning of Total and Local Energies in Elemental Boron

Volker L. Deringer,<sup>1,2,\*</sup> Chris J. Pickard,<sup>3,4</sup> and Gábor Csányi<sup>1</sup><sup>1</sup>*Engineering Laboratory, University of Cambridge, Trumpington Street, Cambridge CB2 1PZ, United Kingdom*<sup>2</sup>*Department of Chemistry, University of Cambridge, Lensfield Road, Cambridge CB2 1EW, United Kingdom*<sup>3</sup>*Department of Materials Science and Metallurgy, University of Cambridge,  
27 Charles Babbage Road, Cambridge CB3 0FS, United Kingdom*<sup>4</sup>*Advanced Institute for Materials Research, Tohoku University 2-1-1 Katahira, Aoba, Sendai, 980-8577, Japan*

(Received 16 October 2017; revised manuscript received 26 January 2018; published 10 April 2018)

The allotropes of boron continue to challenge structural elucidation and solid-state theory. Here we use machine learning combined with random structure searching (RSS) algorithms to systematically construct an interatomic potential for boron. Starting from ensembles of randomized atomic configurations, we use alternating single-point quantum-mechanical energy and force computations, Gaussian approximation potential (GAP) fitting, and GAP-driven RSS to iteratively generate a representation of the element's potential-energy surface. Beyond the total energies of the very different boron allotropes, our model readily provides atom-resolved, local energies and thus deepened insight into the frustrated  $\beta$ -rhombohedral boron structure. Our results open the door for the efficient and automated generation of GAPs, and other machine-learning-based interatomic potentials, and suggest their usefulness as a tool for materials discovery.

DOI: [10.1103/PhysRevLett.120.156001](https://doi.org/10.1103/PhysRevLett.120.156001)

Elemental boron presents a number of complex crystal structures as a direct consequence of its unique and electron-deficient bonding nature [1–3]. This poses formidable challenges for experimentalists and theorists alike. Among the most fundamental is determining the thermodynamically stable ground state between two competing forms:  $\alpha$ -rhombohedral boron, which contains B<sub>12</sub> icosahedra exclusively [4], and  $\beta$ -rhombohedral boron ( $\beta$ -B in the following), which exhibits partial occupations and geometric frustration, most unusual for an elemental ground-state structure [5–9]. The energy difference between the  $\alpha$  and  $\beta$  forms has been studied extensively using density-functional theory (DFT) [8–15] and recently probed by calorimetric experiments [16]; the consensus is now that  $\beta$ -B is indeed more stable at ambient conditions.

In recent years, DFT has played a central role not only in understanding  $\beta$ -B but also in the discovery and structural elucidation of other allotropes. Prominently, a high-pressure structure dubbed  $\gamma$ -B<sub>28</sub> has been determined with the aid of evolutionary crystal-structure searching [17], as well as direct methods [18,19]. Similar techniques have recently identified “borophenes” and other two-dimensional boron allotropes with interesting electronic properties [20–22].

Despite their widespread successes [23], DFT-based structure-searching algorithms are severely restricted by their high computational cost. While excellent empirical interatomic potentials are available today for many solid-state systems, there is a conspicuous lack of such potentials for boron [24]—the single interatomic potential in the literature, as the authors stress, is fitted to quantum-mechanical reference data for  $\alpha$ -boron exclusively [24].

No empirical potential is known to us that could reliably describe the potential-energy surface (PES) of elemental boron applicable to multiple phases.

To overcome the performance and scaling limitations of DFT, machine learning (ML) is increasingly used these days for both creating interatomic potential models [25] and for speeding up structure-searching algorithms [26,27]. Fast ML-based potentials have been suggested to be useful for driving structure searches [28], and indeed, we have shown that a ML potential initially fitted for liquid and amorphous carbon [29] can be used to discover hitherto unknown hypothetical carbon allotropes [30]. However, many carbon (as well as silicon) networks can readily be generated by direct enumeration [31–33]. It would now be interesting to apply ML-driven searches to a system with more complex structure and bonding, for which boron is an ideal and challenging test case.

In this Letter, we demonstrate how a ML-based interatomic potential can be systematically constructed by the iterative exploration of configuration space without prior knowledge of any local minima. It was recently shown that evolutionary searches provide diverse and representative input structures for fitting ML potentials [34], but here, we take this concept further by searching “on the fly” [35–37]; our structure search is driven not by DFT but by the ML model itself, and it generates input data for the next iteration of ML training; this is repeated until a “consistent” model is achieved, i.e., one that does not generate new structures that significantly alter the potential when added to the training set. Therefore, the searching is neither done *ex post*, as in our previous work that used an existing GAP

[30], nor merely as a means to an end, but here it is the central technique we use for exploring and fitting a complex PES.

We start our search from an ensemble of randomized periodic structures, similar in spirit to the *ab initio* random structure searching (AIRSS) technique [38,39]. Our protocol includes two components. First, we generate random structures with 2–32 individual atoms per unit cell corresponding to a wide range of densities, aiming for a comprehensive sampling of the PES including higher-energy regions. Second, we generate structures with either 8 or 12 at./cell that are repeated by 1–4 space-group symmetry operations, and an initial density more closely centered around that of  $\alpha$ -B<sub>12</sub>; such a more constrained input is closer to what would typically be used in AIRSS. We stress that  $\alpha$ -B<sub>12</sub>, or other known crystalline forms, do not enter our fit at this time, and indeed, being able to find  $\alpha$ -B<sub>12</sub> “from scratch” is a challenging and crucial proof for the transferability of the potential (vide infra).

We generated 500 random structures with each of these two approaches, and we used single-point DFT-PBE computations [40] to obtain their energies and forces. These reference data were generated using dense spacing of  $k$  meshes (0.02 Å<sup>-1</sup>), a plane-wave cutoff energy of 800 eV, and on-the-fly pseudopotentials as implemented in CASTEP 8.0 [41]. The resulting energies are shown in Fig. 1(a) as light green points.

The first (and less constrained) approach yields highly scattered results, as expected, and the unrelaxed trial structures have a median energy of 6.1 eV/at. above  $\alpha$ -B<sub>12</sub>. The other seeding procedure gives 1.3 eV/at., and the resulting structures lie much closer together in the  $E$ - $V$  plot [Fig. 1(a)]. Normally, one would now relax these structures using DFT [34,39]. Instead, we show in the following how single-point computations are sufficient to initialize a model that then progressively explores lower-lying configurations without prior knowledge of existing crystal structures.

To “machine-learn” the PES spanned by these seed points, we fitted a Gaussian approximation potential (GAP) model [42] using a systematic protocol for combining properly scaled two-, three-, and many-body descriptors and a radial cutoff of 3.7 Å. This is similar to previous work where details of the approach may be found [29]. In particular, we encode many-body interactions using the smooth overlap of atomic environments (SOAP) kernel [43], the only modification being a properly chosen smoothness parameter as described below.

With the initial potential available (denoted “generation 0” in the following), we performed random structure searching, creating new seeds as above but now relaxing them using GAP. We therefore call this technique “GAP-RSS.” In all GAP-RSS searches, we applied randomized external pressure values, drawn from an exponential distribution with a width of 100 GPa and a rate

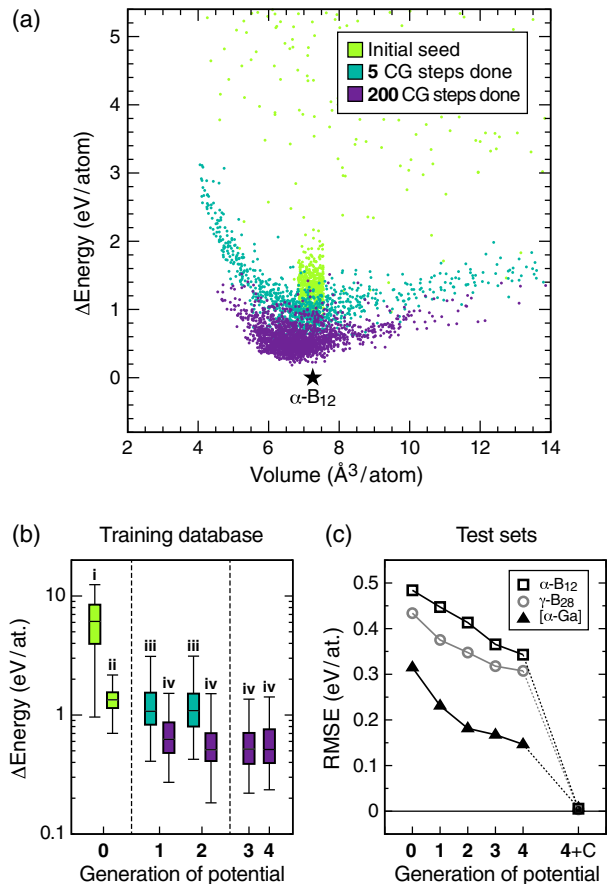


FIG. 1. The iterative construction of a machine-learning model for the potential-energy surface of boron. (a) An energy–volume plot for the training database of DFT reference computations. Starting with an initial seed of random structures (light green), we iteratively generate new seeds and relax them using the previous generation of the GAP, adding data points after 5 (teal) and up to 200 (purple) conjugate-gradient (CG) steps. The optimized  $\alpha$ -B<sub>12</sub> structure is set as the energy zero. (b) The evolution of DFT energies in the progressively generated database, for (i) less constrained and (ii) more constrained initial seed structures; (iii) GAP-RSS snapshots after 5 CG steps; (iv) the same after up to 200 CG steps; see text for details. Boxes denote percentiles corresponding to one standard deviation (68%); bold horizontal lines denote the median, and whiskers the entire range of data. (c) RMSE energy errors for test sets of distorted crystal structures with small unit cells. After step 4, these crystal structures were added to the database (“+C”).

parameter of  $\lambda = 5$ , to sample more densely packed structures. We took snapshots of these relaxations after 5 and up to 200 conjugate-gradient steps, respectively: the former sample the early stages of relaxation trajectories, and the latter are close to the local minima. The results of single-point DFT computations on these snapshots were added to the database after each iteration [Fig. 1(a)–1(b)]. We performed this process twice (generation 1–2), and then added two generations, feeding back only local minima (3–4), after which the distribution of energies in the training database was deemed to be converged [Fig. 1(b)].

While our protocol deliberately starts without knowledge of the crystalline phases, we show that it can indeed progressively “learn” their total energies. In Fig. 1(c), we test the prediction error for the three phases with well-defined unit cells, and we find that this error is continuously improved with the growing size of the reference database. The  $\alpha$ -B<sub>12</sub> structure shows the largest total-energy error among the three, which seems intuitive given the quite unique structural feature of B<sub>12</sub> icosahedra linked by short intericosahedral bonds. We furthermore performed “diagnostic” GAP-RSS runs, using 5,000 attempts with 12 at./cell and a limited set of symmetry operations, and all of these correctly returned the  $\alpha$ -B<sub>12</sub> structure one or more times. In other words, even the zeroth-generation model can identify this challenging structure in principle. Therefore, after generation 4, we chose to add data for distorted unit cells of the known crystal structures to the training database (“4 + C”)—as expected, this reduces the RMSE to very close to zero [Fig. 1(c)].

The final database contains the results of 5,038 single-point computations (corresponding to over 97,000 individual atomic environments). We emphasize again that only single point DFT calculations were performed; no sampling or searching was done with DFT.

We found that the results of our procedure depend on the smoothness of the potential, which is controlled by a single parameter,  $\sigma_{\text{at}}$ , in the SOAP formalism [43]. A setting of  $\sigma_{\text{at}} = 0.5 \text{ \AA}$  was previously used successfully to fit GAP models for carbon [29] and tungsten [44], but it did not produce stable potentials for early-generation GAP-RSS minimizations in our experiments. A smoother potential is required to interpolate between the high-energy data points at the early stages of GAP-RSS, while still being accurate enough for finding local minima at all. We found  $\sigma_{\text{at}} = 0.75 \text{ \AA}$  to be a viable choice for structure searching and used this throughout the iterations, together with  $n_{\text{max}} = l_{\text{max}} = 8$  for the spherical-harmonics expansion of the neighbor density in SOAP (as described in Ref. [43]). Once the database was completed, we performed a final fit on the same database but with tighter settings of  $\sigma_{\text{at}} = 0.5 \text{ \AA}$  and  $n_{\text{max}} = l_{\text{max}} = 12$ .

To validate our potential, we computed DFT energies at varied unit-cell volumes for the most important boron allotropes [17], viz.  $\alpha$ -B<sub>12</sub>,  $\gamma$ -B<sub>28</sub>, a high-pressure  $\alpha$ -Ga type polymorph, and  $\beta$ -B. To represent the disordered structure of the latter, we use the discrete “ $\beta$ -B<sub>106</sub>” structural model (see below) that provides a good approximant of the experimentally determined mixed occupations and is practically degenerate with  $\alpha$ -B<sub>12</sub> in DFT energy [12]. Indeed, Fig. 2 illustrates immediately why the PES of boron is such a challenging case: the energy differences between three polymorphs containing B<sub>12</sub> units are tiny, and only the fundamentally different [ $\alpha$ -Ga] structure (not containing any B<sub>12</sub> icosahedra) is clearly distinct from the other polymorphs on this energy scale. Still, our final GAP

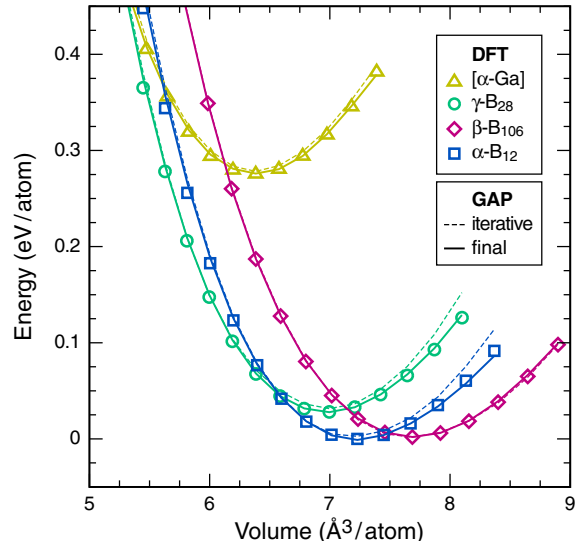


FIG. 2. The energy–volume plots for boron allotropes. The symbols denote the results of DFT computations, whereas lines connect GAP energies for the same structures. Two versions of the potential have been fitted to the complete reference database: one (dashed lines) using the smooth settings as in the iterative protocol, and one (thick lines) with the final, tighter settings.

reproduces the energy of all these structures extremely well (Fig. 2).

As a further test, we generated discrete trial structures with site occupations that are not part of the training (Fig. 3): recall that our reference database does contain  $\beta$ -B, but it describes it using only one particular set of occupations ( $\beta$ -B<sub>106</sub>). Here, by contrast, we started from the most detailed structural model available, which was proposed based on single-crystal x-ray diffraction from a highly pure sample (carbon impurities  $\approx 150$  ppm) [7]. Besides the known B13 and B16 sites (which have previously reported site occupations of approximately 3/4 and 1/4, respectively; Ref. [6]), this model contains additional partially occupied sites, labeled B17–B20, with occupations of just a few percent [7]. We randomly generated ten structures, each containing 321 atoms in hexagonal cell setup, as a representative of the partial occupancies observed experimentally. None of these discrete structures had been included in the GAP fitting, and so they provide another benchmark for the potential. Again, the GAP result is in very good agreement with DFT.

We finally show how a common feature of interatomic potentials can here be turned into a distinct advantage. Interatomic potentials for materials, by their essential nature and similarly to biomolecular force fields, are typically a combination of terms for long-range interactions (describing electrostatics and dispersion) and short-range (often called “bonded”) interactions [25]. We focus here on the latter, which can be understood as a decomposition the total energy  $E$  of a collection of atoms into a sum of atomic contributions,  $E = \sum_i \epsilon_i$ , where the local atomic energy  $\epsilon_i$

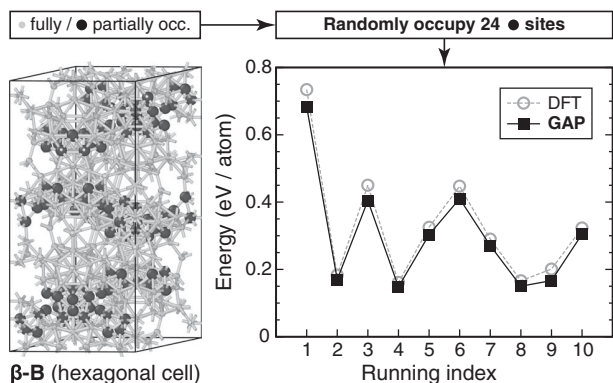


FIG. 3. The stability of randomized mixed-occupation models for  $\beta$ -B as a test for the transferability of the potential. The structural drawing shows the hexagonal unit-cell setup according to Ref. [7]; fully occupied Wyckoff sites are indicated by small, light gray atoms, whereas partially occupied sites are shown by larger, black atoms. On the latter sites, we randomly distribute 24 B atoms, which, together with 297 atoms on fully occupied sites, constitute the  $\beta$ -B<sub>321</sub> model. The right-hand side shows energies for ten arbitrary, discrete structural models created in this fashion, computed using DFT and the final version of our GAP, respectively.

depends only on a region around the  $i$ -th atom as specified by a cutoff radius (here,  $r_{\text{cut}} = 3.7 \text{ \AA}$ ). While this intrinsically limits the attainable accuracy of the potential (since quantum mechanics is fundamentally long-ranged) [29,42], this approximation is often rather good, and here, it allows us to analyze the local stability of atoms—which otherwise is not straightforwardly possible within a quantum-mechanical framework. This is particularly interesting for  $\beta$ -B.

Figure 4(a) shows GAP-computed local energies  $\varepsilon_i$  for individual atoms in a characteristic fragment from  $\beta$ -B, described using the simplistic  $\beta$ -B<sub>105</sub> model without any partial occupations [45]. Besides icosahedral B<sub>12</sub> units, this structure contains B<sub>28</sub> building blocks that can be regarded as triply fused icosahedra. Figure 4(a) shows two such complete clusters, connected to an isolated atom (B15) at the center of the unit cell, via three apical atoms (B13) each. However, the latter site has been shown to be only partially occupied [5–7], and the GAP analysis corroborates this: a full occupation of the B13 sites is clearly unfavorable due to high local energies (red).

Indeed, a more favorable structural model is obtained when only five of six B13 sites are occupied [Fig. 4(b)] [12], in accord with the more recent structural refinements in the experimental literature [5–7]. In this case, which corresponds to the  $\beta$ -B<sub>106</sub> model used in Fig. 2, the local energies of the remaining two B13 atoms are significantly lowered. Vacancy formation also stabilizes the central B15 atom. In turn, one of the constituent icosahedra is now defective due to the presence of a vacancy ( $\square$ ), and therefore, the neighboring atoms have higher local energies (pale red) than those in the complete fragment above

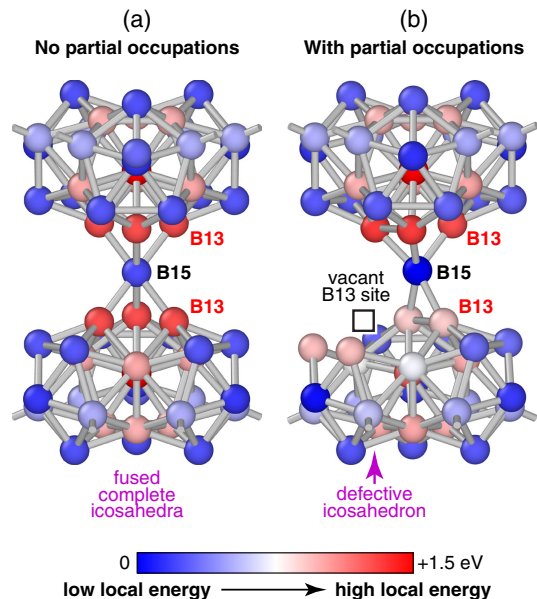


FIG. 4. A local energy analysis using our GAP, comparing the simplistic  $\beta$ -B<sub>105</sub> model without partial occupations (a) to the more disordered and favorable  $\beta$ -B<sub>106</sub> model (b). The characteristic fragment at the center of the  $\beta$ -B unit cell is shown, with atoms color coded according to more favorable (blue) to less favorable (red) environments. Crystallographic sites are labeled as in the original literature; the analysis was performed for optimized structures. Visualization was done using OVITO [46]. Note that while a vacancy has been created locally, the structural model in (b) contains one more atom per unit cell overall, due to the additional occupation of B16 sites (not shown).

(blue). Future work will deal with a more quantitative treatment of different mixed occupations, in the spirit of Ref. [8], but now using GAP.

In conclusion, we have generated an interatomic potential for elemental boron that describes the energetics of multiple polymorphs by unifying ideas from machine-learning potential fitting and random structure searching. We have shown that it is possible to explore and fit a challenging potential-energy surface at the same time. Our protocol requires single-point DFT calculations only, and therefore, it can explore configuration space with reasonable computational effort. We used the Gaussian approximation potential framework for fitting here, but other methods, such as artificial neural networks, can be combined with the same ideas. Our next methodological efforts will attempt to integrate selected results of large searches (such as the 5,000 attempts mentioned above) directly into the iterations that construct the potential. This way, we envision that it should be ultimately possible to “learn” significant crystal structures in a fully automatic fashion. In the long run, this is expected to enable the routine construction of interatomic potentials of unprecedented quality and flexibility for the purpose of materials discovery.

Data supporting this publication are available at [47].

We thank N. Bernstein, S. R. Elliott, and D. M. Proserpio for ongoing valuable discussions and collaborations and the referees for constructive criticism. V. L. D. gratefully acknowledges a Feodor Lynen fellowship from the Alexander von Humboldt Foundation, a Leverhulme Early Career Fellowship, and support from the Isaac Newton Trust. C. J. P. is supported by the Royal Society through a Royal Society Wolfson Research Merit award. This work used the ARCHER UK National Supercomputing Service via EPSRC Grants No. EP/K014560/1 and No. EP/P022596/1.

\* vld24@cam.ac.uk

- [1] B. Albert and H. Hillebrecht, *Angew. Chem., Int. Ed. Engl.* **48**, 8640 (2009).
- [2] A. R. Oganov and V. L. Solozhenko, *J. Superhard Mater.* **31**, 285 (2009).
- [3] T. Ogitsu, E. Schwegler, and G. Galli, *Chem. Rev.* **113**, 3425 (2013).
- [4] L. V. McCarty, J. S. Kasper, F. H. Horn, B. F. Decker, and A. E. Newkirk, *J. Am. Chem. Soc.* **80**, 2592 (1958).
- [5] J. L. Hoard, D. B. Sullenger, C. H. L. Kennard, and R. E. Hughes, *J. Solid State Chem.* **1**, 268 (1970).
- [6] B. Callmer, *Acta Crystallogr. Sect. B* **33**, 1951 (1977).
- [7] G. A. Slack, C. I. Hejna, M. F. Garbaskas, and J. S. Kasper, *J. Solid State Chem.* **76**, 52 (1988).
- [8] T. Ogitsu, F. Gygi, J. Reed, Y. Motome, E. Schwegler, and G. Galli, *J. Am. Chem. Soc.* **131**, 1903 (2009).
- [9] T. Ogitsu, F. Gygi, J. Reed, M. Udagawa, Y. Motome, E. Schwegler, and G. Galli, *Phys. Rev. B* **81**, 020102(R) (2010).
- [10] D. L. V. K. Prasad, M. M. Balakrishnarajan, and E. D. Jemmis, *Phys. Rev. B* **72**, 195102 (2005).
- [11] A. Masago, K. Shirai, and H. Katayama-Yoshida, *Phys. Rev. B* **73**, 104102 (2006).
- [12] M. J. van Setten, M. A. Uijtewaald, G. A. de Wijs, and R. A. de Groot, *J. Am. Chem. Soc.* **129**, 2458 (2007).
- [13] M. Widom and M. Mihalkovič, *Phys. Rev. B* **77**, 064113 (2008).
- [14] B. Siberchicot, *Phys. Rev. B* **79**, 224101 (2009).
- [15] Q. An, K. M. Reddy, K. Y. Xie, K. J. Hemker, and W. A. Goddard, *Phys. Rev. Lett.* **117**, 085501 (2016).
- [16] M. A. White, A. B. Cerqueira, C. A. Whitman, M. B. Johnson, and T. Ogitsu, *Angew. Chem., Int. Ed. Engl.* **54**, 3626 (2015).
- [17] A. R. Oganov, J. Chen, C. Gatti, Y. Ma, Y. Ma, C. W. Glass, Z. Liu, T. Yu, O. O. Kurakevych, and V. L. Solozhenko, *Nature (London)* **457**, 863 (2009).
- [18] E. Yu. Zarechnaya, L. Dubrovinsky, N. Dubrovinskaia, Y. Filinchuk, D. Chernyshov, V. Dmitriev, N. Miyajima, A. El Goresy, H. F. Braun, S. Van Smaalen, I. Kantor, A. Kantor, V. Prakapenka, M. Hanfland, A. S. Mikhaylushkin, I. A. Abrikosov, and S. I. Simak, *Phys. Rev. Lett.* **102**, 185501 (2009).
- [19] S. Mondal, S. van Smaalen, A. Schönleber, Y. Filinchuk, D. Chernyshov, S. I. Simak, A. S. Mikhaylushkin, I. A. Abrikosov, E. Zarechnaya, L. Dubrovinsky, and N. Dubrovinskaia, *Phys. Rev. Lett.* **106**, 215502 (2011).
- [20] X.-F. Zhou, X. Dong, A. R. Oganov, Q. Zhu, Y. Tian, and H.-T. Wang, *Phys. Rev. Lett.* **112**, 085502 (2014).
- [21] A. J. Mannix, X.-F. Zhou, B. Kiraly, J. D. Wood, D. Alducin, B. D. Myers, X. Liu, B. L. Fisher, U. Santiago, J. R. Guest, M. J. Yacaman, A. Ponce, A. R. Oganov, M. C. Hersam, and N. P. Guisinger, *Science* **350**, 1513 (2015).
- [22] F. Ma, Y. Jiao, G. Gao, Y. Gu, A. Bilic, Z. Chen, and A. Du, *Nano Lett.* **16**, 3022 (2016).
- [23] *Modern Methods of Crystal Structure Prediction*, edited by A. R. Oganov (Wiley-VCH, Weinheim, 2011).
- [24] P. Pokatashkin, A. Kuksin, and A. Yanilkin, *Model. Simul. Mater. Sci. Eng.* **23**, 045014 (2015).
- [25] For a recent overview, see J. Behler, *J. Chem. Phys.* **145**, 170901 (2016).
- [26] T. Yamashita, N. Sato, H. Kino, T. Miyake, K. Tsuda, and T. Oguchi, *Phys. Rev. Mater.* **2**, 013803 (2018).
- [27] T. L. Jacobsen, M. S. Jørgensen, and B. Hammer, *Phys. Rev. Lett.* **120**, 026102 (2018).
- [28] P. E. Dolgirev, I. A. Kruglov, and A. R. Oganov, *AIP Adv.* **6**, 085318 (2016).
- [29] V. L. Deringer and G. Csányi, *Phys. Rev. B* **95**, 094203 (2017).
- [30] V. L. Deringer, G. Csányi, and D. M. Proserpio, *Chem-PhysChem* **18**, 873 (2017).
- [31] R. T. Strong, C. J. Pickard, V. Milman, G. Thimm, and B. Winkler, *Phys. Rev. B* **70**, 045101 (2004).
- [32] R. Hoffmann, A. A. Kabanov, A. A. Golov, and D. M. Proserpio, *Angew. Chem., Int. Ed. Engl.* **55**, 10962 (2016).
- [33] L.-A. Jantke, S. Stegmaier, A. J. Karttunen, and T. F. Fässler, *Chem. Eur. J.* **23**, 2734 (2017).
- [34] S. Hajinazar, J. Shao, and A. N. Kolmogorov, *Phys. Rev. B* **95**, 014114 (2017).
- [35] This is conceptually reminiscent of, but different in detail from, recently proposed schemes to “machine-learn” forces on the fly during MD simulations [36,37].
- [36] Z. Li, J. R. Kermode, and A. De Vita, *Phys. Rev. Lett.* **114**, 096405 (2015).
- [37] E. V. Podryabinkin and A. V. Shapeev, *Comput. Mater. Sci.* **140**, 171 (2017).
- [38] C. J. Pickard and R. J. Needs, *Phys. Rev. Lett.* **97**, 045504 (2006).
- [39] C. J. Pickard and R. J. Needs, *J. Phys. Condens. Matter* **23**, 053201 (2011).
- [40] J. P. Perdew, K. Burke, and M. Ernzerhof, *Phys. Rev. Lett.* **77**, 3865 (1996).
- [41] S. J. Clark, M. D. Segall, C. J. Pickard, P. J. Hasnip, M. J. Probert, K. Refson, and M. C. Payne, *Z. Kristallogr.* **220**, 567 (2005).
- [42] A. P. Bartók, M. C. Payne, R. Kondor, and G. Csányi, *Phys. Rev. Lett.* **104**, 136403 (2010).
- [43] A. P. Bartók, R. Kondor, and G. Csányi, *Phys. Rev. B* **87**, 184115 (2013).
- [44] W. J. Szlachta, A. P. Bartók, and G. Csányi, *Phys. Rev. B* **90**, 104108 (2014).
- [45] D. Geist, R. Kloss, and H. Föllner, *Acta Crystallogr. Sect. B* **26**, 1800 (1970).
- [46] A. Stukowski, *Model. Simul. Mater. Sci. Eng.* **18**, 015012 (2010).
- [47] <http://www.libatoms.org>.